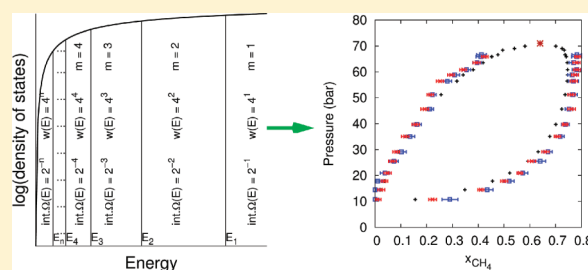


# Calculation of Partition Functions and Free Energies of a Binary Mixture Using the Energy Partitioning Method: Application to Carbon Dioxide and Methane

Hainam Do,\* Jonathan D. Hirst, and Richard J. Wheatley

School of Chemistry, University of Nottingham, University Park, Nottingham, NG7 2RD, United Kingdom

**ABSTRACT:** It is challenging to compute the partition function ( $Q$ ) for systems with enormous configurational spaces, such as fluids. Recently, we developed a Monte Carlo technique (an energy partitioning method) for computing  $Q$  [*J. Chem. Phys.* **2011**, *135*, 174105]. In this paper, we use this approach to compute the partition function of a binary fluid mixture (carbon dioxide + methane); this allows us to obtain the Helmholtz free energy ( $F$ ) via  $F = -k_B T \ln Q$  and the Gibbs free energy ( $G$ ) via  $G = F + pV$ . We then utilize  $G$  to obtain the coexisting mole fraction curves. The chemical potential of each species is also obtained. At the vapor–liquid equilibrium condition, the chemical potential of methane significantly increases, while that of carbon dioxide slightly decreases, as the pressure increases along an isotherm. Since  $Q$  is obtained from the density of states, which is independent of the temperature, equilibrium thermodynamic properties at any condition can be obtained by varying the total composition and volume of the system. Our methodology can be adapted to explore the free energies of other binary mixtures in general and of those containing  $\text{CO}_2$  in particular. Since the method gives access to the free energy and chemical potentials, it will be useful in many other applications.



## 1. INTRODUCTION

Knowing the free energy allows many physical and chemical phenomena to be predicted. The calculation of free energy from theory has been an active field for many decades, yet remains a challenging problem. Methods such as free energy perturbation theory<sup>1–3</sup> and thermodynamic integration<sup>3,4</sup> are frequently used to determine the free energy difference between two states (states I and II for example), and rely on calculations along a path from state I to state II. These states can be characterized by either different potential energy functions or different structures. Systems where states I and II are far apart, with large and complex changes in structure, can require a complicated path between states and can be prohibitively expensive in terms of computing effort. Thus, it is important to develop methods that can provide the free energy for each state I and II independently; in this case, the free energy difference can be calculated even for significantly different states because the integration path is avoided. Methods such as minima mining,<sup>5–7</sup> hypothetical scanning,<sup>8–11</sup> harmonic reference state,<sup>12,13</sup> and nondynamic growth<sup>14–16</sup> have made promising progress toward this goal. However, the efficiency of these techniques deteriorates rapidly with the size and the complexity of the system.

Elegant approaches for calculating free energies via the density of states have been developed in the past few decades, including umbrella sampling,<sup>17</sup> the weighted histogram analysis method (WHAM),<sup>18,19</sup> transition matrix,<sup>20</sup> muticanonical,<sup>21</sup> and Wang–Landau<sup>22</sup> sampling. The idea behind these techniques is either to perform multiple simulations, whose

samplings overlap in configurational space and connect them together (reweight) or to perform the simulations in biased ensembles to achieve broader sampling of particular states that are rarely visited. If the Wang–Landau technique is employed for systems with an infinite energy range, such as fluids, one often has to choose a finite range of energy (cutting off the high-energy range) either via trial and error or by calculation.<sup>23–26</sup> WHAM also uses a finite range of energies. Restricting the density of states to a finite energy range means that the partition function can only be computed to within a multiplicative constant.

To circumvent these limitations, we have recently developed an “energy partitioning” Monte Carlo (MC) technique,<sup>27</sup> which can calculate the “absolute” density of configurational energy states with no high-energy cutoff, from which the excess partition function, and hence the excess free energy of a molecular fluid, can be obtained. The absolute free energy can be calculated by adding the ideal gas free energy to the excess free energy.

Phase equilibrium properties of model systems and real fluids are of tremendous importance to scientists and engineers. Since the measurement of phase equilibrium properties is time consuming and expensive, computer simulation based on molecular modeling is a promising alternative. Free energy can be used to predict the vapor–liquid equilibrium properties and

Received: December 16, 2011

Revised: March 15, 2012

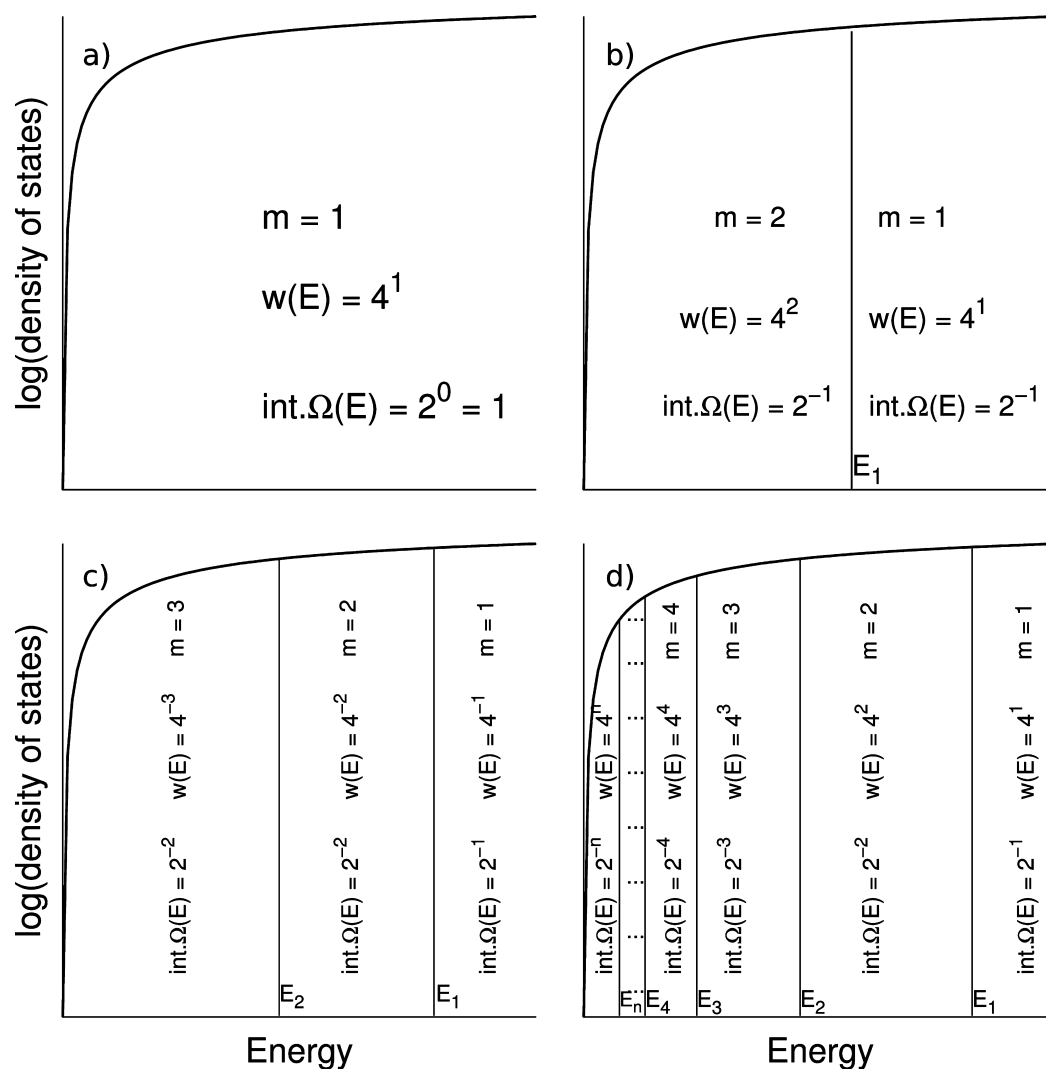


**Figure 1.** Sketch (not to scale) explaining the partitioning of the density of states (a) at the start of the simulation, where there is only one energy subdivision; (b) after placing the first energy boundary; (c) after placing the second energy boundary; and (d) after placing the  $n$ th energy boundary.  $w(E)$  is the weighting function and  $\text{int.}\Omega(E)$  is the integrated normalized density of states.

many other thermodynamic properties, including critical phenomena and  $pVT$  data for single phases. Of particular interest to us are mixtures that contain carbon dioxide ( $\text{CO}_2$ ).<sup>28–33</sup> Systems of  $\text{CO}_2$  in multicomponent mixtures with light paraffins are important to the natural gas industry, since it has become common practice to process gas streams with moderate to high levels of  $\text{CO}_2$ . Supercritical  $\text{CO}_2$  is a novel solvent that has attracted much attention.<sup>34</sup> A property of interest is the unusually high solubility of fluorinated hydrocarbons in supercritical  $\text{CO}_2$ . Mixtures of hydrofluorocarbons and  $\text{CO}_2$  are possible replacements for ozone-depleting refrigerants. Thus, knowledge of the phase equilibrium properties of these mixtures can help optimize their performance in industrial processes.<sup>35</sup>

In this paper, we calculate the partition function and free energy of the binary mixture  $\text{CO}_2 + \text{CH}_4$ . Mixtures of  $\text{CO}_2$  with other small molecules (and other binary mixtures) can be studied analogously. Using the free energy, the vapor–liquid equilibrium properties and the critical points of the mixture are calculated. The chemical potentials of each species are extracted from the free energy. The critical point is observed from a plot of the Helmholtz free energy versus volume.

The paper is organized as follows. In section 2, we describe the theoretical background of the energy partitioning approach. In section 3, we outline the simulation procedure. In section 4, we present results for the partition function, free energy, and vapor–liquid equilibrium properties of the  $\text{CO}_2 + \text{CH}_4$  mixture. We obtain the vapor–liquid equilibrium properties from the free energies, and compare our results with experimental data. We also compare our results with a conventional MC (Gibbs ensemble) simulation technique and demonstrate the advantages of our method compared to this approach. Finally, in section 5, we give concluding remarks and outline future work.

## 2. METHOD

**2.1. Free Energy and Partition Function.** The free energy of a system in the canonical ensemble is given by  $F = -k_B T \ln Q(N, V, T)$ , where  $Q(N, V, T)$  is the partition function of the system, which is the integral of the Boltzmann factor  $\exp(-\beta E)$  over particle positions ( $\mathbf{r}^N$ ) and momenta ( $\mathbf{p}^N$ ). As

the integration over particle momenta can be solved exactly, the canonical partition function can be expressed as

$$Q(N, V, T) = \frac{1}{N! \Lambda^{3N}} \int \exp[-\beta E(\mathbf{r}^N)] d\mathbf{r}^N \quad (1)$$

where  $N$  is the number of particles in the system. The factor  $1/N!$  comes from the fact that particles are indistinguishable,  $\Lambda$  is the thermal de Broglie wavelength,  $E$  is configurational energy,  $\beta$  is  $1/k_B T$ ,  $k_B$  is the Boltzmann constant, and  $T$  is the temperature of the system. Unlike other equilibrium thermodynamic properties, such as the internal energy, that can be estimated as a time or ensemble average, the Helmholtz free energy  $F$  is related directly to the volume of the configurational space (as shown in eq 1), and calculating  $F$  still remains a challenge in molecular simulation.

Equation 1 can be rewritten in the form of reduced coordinates ( $\mathbf{s} = \mathbf{r}/L$ ) as

$$Q(N, V, T) = \frac{V^N}{N! \Lambda^{3N}} \int_0^1 \exp[-\beta E(\mathbf{s}^N)] d\mathbf{s}^N \quad (2)$$

where  $L$  is the length of the cubic simulation box, which contains  $N$  molecules, and  $V$  is the volume of the box. The term  $V^N/(N! \Lambda^{3N})$  in eq 2 is the translational partition function of an ideal gas and can be calculated analytically. Thus, we seek to compute the “excess” part of the partition function ( $Q_{\text{ex}}$ )

$$Q_{\text{ex}} = \int_0^1 \exp[-\beta E(\mathbf{s}^N)] d\mathbf{s}^N \quad (3)$$

The probability of finding an energy  $E$  is proportional to the density of states,  $\Omega(E)$ , where  $\Omega(E) = \int_0^1 \delta(E - E(\mathbf{s}^N)) d\mathbf{s}^N$ . Thus,  $Q_{\text{ex}}$  can be expressed more conveniently as

$$Q_{\text{ex}} = \frac{\int_{-\infty}^{\infty} \exp(-\beta E) \Omega(E) dE}{\int_{-\infty}^{\infty} \Omega(E) dE} \quad (4)$$

where the integral is over all possible energies of the system. Equation 4 shows that if the density of states is known, the excess partition function can be calculated from it. Our goal is to calculate the density of states and hence  $Q_{\text{ex}}$ .

**2.2. Calculation of the Density of States.** The aim of the energy partitioning method is to divide the energy range recursively into subdivisions (indexed  $m$ ), such that the integrated normalized density of states  $\int_{E_{m-1}}^{E_m} \Omega(E) dE / \int_{-\infty}^{\infty} \Omega(E) dE$  is  $1/2^1$  for the first energy subdivision ( $m = 1$ ,  $E_1 \leq E \leq E_0$ ,  $E_0 = \infty$ ) (Figure 1d),  $1/2^2$  for the second subdivision ( $m = 2$ ,  $E_2 \leq E \leq E_1$ ), and so on down to  $1/2^n$  for the two lowest-energy subdivisions ( $m = n$ ,  $E_n \leq E \leq E_{n-1}$  and  $m = n + 1$ ,  $-\infty \leq E \leq E_n$ ).

At the start of the simulation, there is only one energy subdivision (Figure 1a). All MC moves are accepted at this stage (random sampling), and the sampled energies are saved. After a predetermined number of MC moves (usually several thousand), the energy range  $-\infty \leq E \leq \infty$  is divided: the first energy boundary  $E_1$  is set equal to the median configurational energy. The choice of the number of MC steps used in each division of the energy is explained in section 3. After the first division of the energy (Figure 1b), there are two energy subdivisions with the same integrated density of states ( $1/2$  and  $1/2$ ). We then throw away all the sampled energies and move on to the second division of the energy.

During the second division of the energy (Figure 1b), MC moves are accepted based on a biased weighting function  $w(E) = 4^m$ , where  $m$  is the energy subdivision into which the configurational energy  $E$  falls so the weighting functions for the energy subdivisions 1 ( $E > E_1$ ) and 2 ( $E \leq E_1$ ) are  $4^1$  and  $4^2$ , respectively. These biased weighting functions are necessary to push the system toward the low-energy region; the energy subdivision 2 is visited four times as often on average as the energy subdivision 1. After the same predetermined number of MC moves as above, the second energy boundary  $E_2$  is set equal to the median configurational energy found in the lowest-energy subdivision  $-\infty \leq E \leq E_1$ . This produces three energy subdivisions with the integrated density of states equal to  $1/2$ ,  $1/4$ , and  $1/4$  for the highest energy, middle, and lowest energy, respectively (Figure 1c). Then the sampled energies are discarded once again and the third division of the energy starts.

During the third division of the energy (Figure 1c), the weighting for each energy subdivision is  $4^1$ ,  $4^2$ , and  $4^3$  for the highest-energy, middle, and lowest-energy subdivision respectively, which means that the lowest-energy subdivision (subdivision 3) is visited four and eight times as often on average as the subdivisions 2 and 1 respectively. At the end of the MC procedure, the third energy boundary  $E_3$  is set equal to the median configurational energy found in the lowest-energy subdivision  $-\infty \leq E \leq E_2$ . There are now four energy subdivisions with the integrated density of states equal to  $1/2$ ,  $1/4$ ,  $1/8$ , and  $1/8$  for the highest-energy to the lowest-energy subdivisions respectively.

The procedure continues iteratively. In general, for the  $n$ th division of the density of states (to produce energy boundary  $E_n$ ,  $n \geq 2$ ), MC sampling is performed with a weighting function  $w(E) = 4^m$  for the previously calculated subdivisions,  $1 \leq m \leq n$  (subdivision 1 being the highest energy). The weighting function is essential to speed up the simulations; it ensures that about  $2/3$  or more of the configurations of the system fall into the current lowest-energy subdivision.<sup>27</sup> The probability of accepting a move from an old state with configurational energy  $E_{\text{old}}$  that falls into subdivision  $m_{\text{old}}$  to a new state with configurational energy  $E_{\text{new}}$  that falls into subdivision  $m_{\text{new}}$  is given by

$$P(\text{old} \rightarrow \text{new}) = \min\left(1, \frac{w(E_{\text{new}})}{w(E_{\text{old}})}\right) = \min\left(1, \frac{4^{m_{\text{new}}}}{4^{m_{\text{old}}}}\right) \quad (5)$$

At the end of the predetermined number of MC moves, the energy boundary  $E_n$  is set equal to the median configurational energy found in the lowest-energy subdivision  $-\infty \leq E \leq E_{n-1}$  and all sampled energies are discarded. The simulation is repeated for the next division of the energy until it is terminated.

The density of states  $\Omega(E)$  strongly increases with energy (except at very high energy),  $\exp(-\beta E)$  strongly decreases with energy, and the function  $\Omega(E) \exp(-\beta E)$ , which is integrated in eq 4 to get  $Q$ , has a maximum at an average energy. Since this average energy is not known, the number of energy boundaries is not fixed in advance. It is found during the simulation using the criterion that when the integrated function  $[\int \Omega(E) \exp(-\beta E) dE]_m$  for the current lowest-energy ( $m$ th) subdivision is much smaller than its maximum value over all energy subdivisions,  $[\int \Omega(E) \exp(-\beta E) dE]_{\text{max}}$ , the simulation can be terminated, as nothing would be gained by further subdividing the density of states. A stopping criterion of

$[\int[\Omega(E) \exp(-\beta E) dE]_m] = 10^{-9}[\int[\Omega(E) \exp(-\beta E) dE]_{\max}]$  is used. This is temperature dependent, and we use the lowest temperature of interest, in order to cover all the important parts of the energy range.

Once the simulation is finished, the excess partition function is obtained from the normalized integrated density of states as (cf. eq 4)

$$Q_{\text{ex}} = \frac{\sum_{m=1}^{m-n+1} (\int_{E_m}^{E_{m-1}} \Omega(E) dE) \exp(-\beta \langle E \rangle_m)}{\sum_{m=1}^{m-n+1} (\int_{E_m}^{E_{m-1}} \Omega(E) dE)}$$

$$= \frac{\sum_{m=1}^{m-n+1} 2^{-m} \exp(-\beta \langle E \rangle_m)}{\sum_{m=1}^{m-n+1} 2^{-m}} \quad (6)$$

where  $\langle E \rangle_m = (E_m + E_{m-1})/2$ . For the first energy subdivision ( $m = 1$ ),  $\langle E \rangle_m$  is set equal to  $E_1$ , and for the last energy subdivision,  $\langle E \rangle_m$  is set equal to  $E_n$ . Also, in the last energy subdivision,  $2^{-m}$  is replaced by  $2^{-n}$ , as the normalized integrated density of states of the two lowest-energy subdivisions are the same and equal to  $2^{-n}$ . Errors produced in this application by introducing  $\langle E \rangle_m$  are negligible. However, more care would be needed if very few energy subdivisions were found.

**2.3. Intermolecular Potentials.** The quality of the results of a computer simulation depends on the potential models describing the interactions between the molecules of the studied substances. Much effort has been devoted to the development of an accurate potential for CO<sub>2</sub>. In our simulations, the rigid fixed-point charge elementary physics model (EPM) is employed, due to its widespread use.<sup>36</sup> In general, one would not expect force fields to predict properties accurately at high pressure. However, the EPM model performs reasonably well under moderately high pressure (<200 bar).<sup>37,38</sup> To enable combination with the CO<sub>2</sub> model, potentials for CH<sub>4</sub> with the same functional form are required. The transferable potentials for phase equilibrium with explicit hydrogen atoms (TraPPE-EH) model<sup>39</sup> is used for CH<sub>4</sub>: the CH<sub>4</sub> molecule has five Lennard-Jones interaction sites, which are located at the carbon atom and the centers of the CH bonds. For Lennard-Jones interactions between unlike atoms, the Lorentz–Berthelot combining rules are used.

### 3. SIMULATION DETAILS

A series of simulations are performed at different total mole fractions and densities to calculate the excess partition functions of the mixture under these conditions. The results are a set of  $Q_{\text{ex}}$  at different compositions ranging from the vapor phase to the liquid phase (passing through the two-phase region). The Gibbs free energy is obtained directly from  $Q_{\text{ex}}$  ( $G = -k_B T \ln Q_{\text{ex}} + pV$ ) and utilized to obtain the coexisting mole fraction curves at constant pressure. More details about this are given in section 4. At the start of each simulation, 300 molecules with the desired total mole fraction are inserted randomly into a cubic periodic box of fixed volume. 45 000 MC steps are employed for each partition of the energy. Each MC step involves either a translational move or a rotational move of a single molecule with the same probability. At the beginning of the simulation, the maximum displacement of a translational move is set to  $L/4$  and that of a rotational move is set to  $180^\circ$ . The acceptance rates of both moves are 100% during the first division of the energy (as implied by the weighting function). They then decrease as the number of energy subdivisions,  $m$ ,

increases. Once  $m$  becomes large enough for the acceptance rates to drop to 30%, the maximum displacements are adjusted automatically after each energy division to keep acceptance rates of about 30% throughout the rest of the simulation.

A spherical cutoff of half of the length of the simulation box is used to truncate the potential energy. Thus, a long-range correction for the dispersion  $r^{-6}$  term (tail correction)<sup>3</sup> is used. The  $r^{-12}$  term decays rapidly with distance, so a correction for this term is unnecessary. The CO<sub>2</sub> and CH<sub>4</sub> molecules are nonpolar; the quadrupole–quadrupole interactions are sufficiently short range that a long-range correction for the electrostatic energy is not needed. This has been examined and confirmed in our previous study on this system.<sup>31</sup>

The efficiency and accuracy of the simulations depend on the choice of the number of MC steps used in each partition of the energy. Fewer MC steps give faster calculations but lower accuracy. Figure 2 shows the effect on the accuracy of the

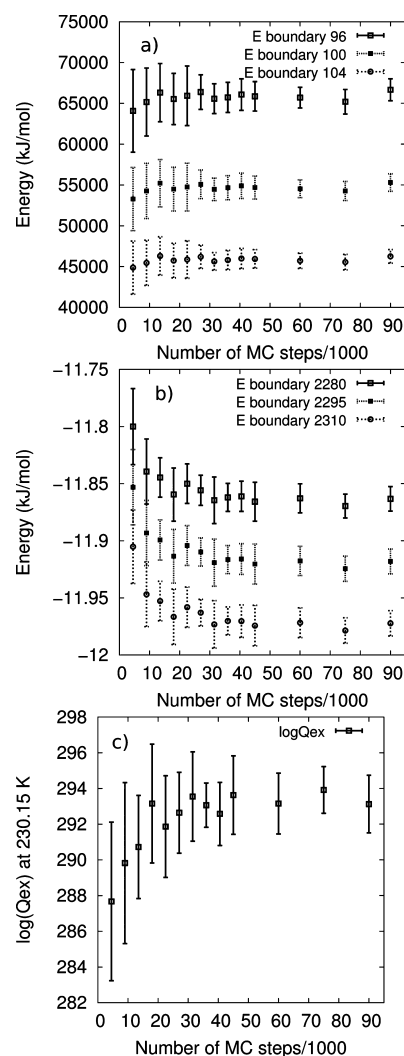


**Figure 2.** Effect on the partitioning method of the number of MC steps used in each partitioning of the energy (50% CO<sub>2</sub> and 50% CH<sub>4</sub> at number density = 0.019 Å<sup>-3</sup>). (a) Errors in selecting the energy boundary in the high-energy region. (b) Errors in selecting the energy boundary in the low-energy region. (c) Errors in the excess partition function (at 230.15 K). The total number of energy subdivisions under these conditions is about 2370. The standard deviations are determined by performing a set of 15 different simulations.

method of the number of MC steps used to determine each energy boundary. In the early state of the partitioning process (the first few hundred partitions), 10 000 or fewer MC steps could be used (Figure 2a), but as the number of energy subdivisions grows, at least 18 000 MC steps are needed, as the simulations take longer to equilibrate (Figure 2b). If fewer than 18 000 MC steps are employed in the low-energy region, a systematic error occurs. The excess partition function is most accurately calculated with at least 18 000 MC steps (Figure 2c). In the rest of this work, 45 000 MC steps are used. To speed up the calculations, fewer MC steps could be used in the high-energy region than in the low-energy region, but we have not investigated this possibility further.

In the first iteration of the simulation, all 45 000 MC steps are in the lowest-energy subdivision, which spans the entire energy range (Figure 1a). In the second iteration, the weighting between the energy subdivision 1 ( $m = 1$ ) and the energy subdivision 2 ( $m = 2$ ) is 1:4 and, therefore, we expect 1/5 of the total MC steps ( $\approx 9000$ ) to be in the high-energy subdivision and 4/5 of the total MC steps ( $\approx 36\,000$ ) in the low-energy subdivision. The energy boundary  $E_2$  is drawn from the  $\approx 36\,000$  MC steps in the low-energy subdivision. In the third iteration, the ratio between the weighting of the energy subdivisions 1, 2, and 3 (lowest-energy) is 1:4:16 and the integrated density of states is 2:1:1. Thus, we expect to collect 2/22 ( $\approx 4091$ ), 4/22 ( $\approx 8182$ ), and 16/22 ( $\approx 32\,727$ ) of the total MC steps in the energy subdivisions 1, 2, and 3, respectively. The energy boundary  $E_3$  is the median configurational energy found in the  $\approx 32\,727$  MC steps in the lowest-energy subdivision. As the number of energy subdivisions increases, about 2/3 ( $\approx 30\,000$ ) MC steps are found in the current lowest-energy subdivision, as dictated by the weighting function, and the energy boundary  $E_n$  is set equal to the median configurational energy found in the lowest-energy subdivision.

#### 4. RESULTS AND DISCUSSION

The calculated density of states is used to obtain the partition function, free energy, vapor–liquid equilibrium properties, and chemical potential of the binary mixture  $\text{CO}_2 + \text{CH}_4$ . After the partitioning process, the entire energy range (for a fixed composition and volume) has been discretized into  $n + 1$  energy subdivisions (see Figure 1). The excess partition function is obtained using eq 6, and the excess Helmholtz free energy ( $F_{\text{ex}}$ ) is calculated using  $F_{\text{ex}} = -k_{\text{B}}T \ln Q_{\text{ex}}$ . The density dependence of the ideal gas free energy ( $F_{\text{id}}$ ) is calculated using  $F_{\text{id}} = k_{\text{B}}T(x_{\text{CO}_2} \ln \rho_{\text{CO}_2} + x_{\text{CH}_4} \ln \rho_{\text{CH}_4})$ , where  $x$  is the mole fraction and  $\rho$  is the number density. The density-dependent part of the absolute free energy is the sum of the excess part and the ideal gas part ( $F = F_{\text{ex}} + F_{\text{id}}$ ). The Gibbs free energy is  $G = F + pV$ , where  $p$  is the pressure and  $V$  is the volume of the system. Figure 3 shows the Gibbs free energy per particle versus volume per particle for  $\text{CO}_2 + \text{CH}_4$  mixtures at 230.15 K, 20.92 bar and 250.15 K, 38.36 bar. This shows the preference for each phase of the system under different conditions. For example, at 230.15 K and 20.92 bar (Figure 3a), the liquid phase is favored (a lower minimum in the free energy) when there is no  $\text{CH}_4$  present. When the mole fraction of  $\text{CH}_4$  is 0.2, two minima are observed, but the liquid phase is still favored. As the total mole fraction of  $\text{CH}_4$  increases, the vapor phase becomes favored. The liquid phase is less favored and disappears when the mole fraction of  $\text{CH}_4$  reaches about 0.6; i.e., the critical composition is reached for this temperature.

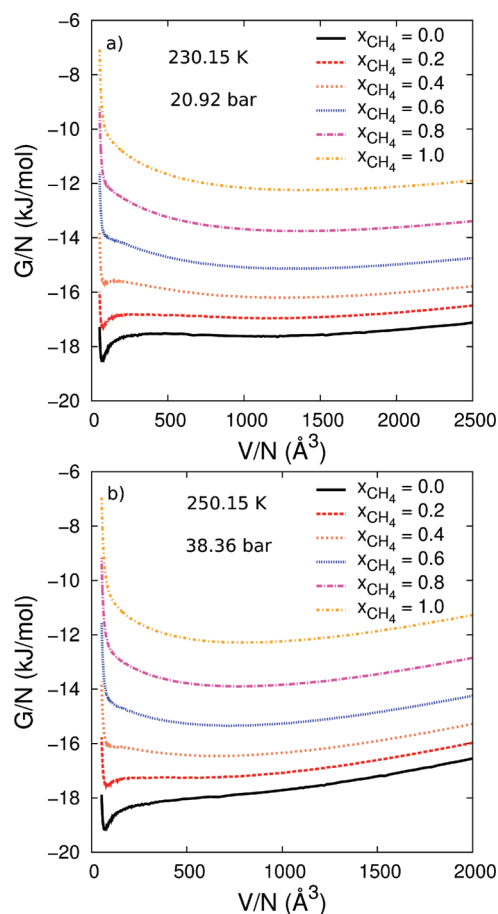


**Figure 3.** Gibbs free energy per particle versus volume per particle of  $\text{CO}_2 + \text{CH}_4$  at different compositions: (a) 230.15 K and 20.92 bar and (b) 250.15 K and 38.36 bar. The standard errors are determined by performing a set of 15 different simulations for each volume. In most cases, the errors in  $G/N$  are between 0.4% and 0.7%. For the sake of clarity, the plots at the compositions of  $\text{CH}_4$  equal to 0.0, 0.2, 0.4, 0.6, and 0.8 are offset by  $-5$ ,  $-3.5$ ,  $-2.5$ ,  $-1.5$ , and  $-0.5$  kJ/mol, respectively.

Similar observations can also be made at other conditions, for example, at 250.15 K and 38.36 bar (Figure 3b).

Using the minima in Figure 3, a plot of the Gibbs free energy versus the composition for both phases is constructed, from which the vapor–liquid equilibrium compositions are determined (Figure 4). The coexisting compositions are determined by constructing a double common tangent connecting both phases. The chemical potential for each species at any composition can be calculated by taking  $G$  and  $dG/dx$  from Figure 4 and solving the simultaneous equations

$$\begin{cases} x_1^\alpha \mu_1^\alpha + x_2^\alpha \mu_2^\alpha = G^\alpha \\ dG^\alpha/dx_1^\alpha = \mu_1^\alpha - \mu_2^\alpha \end{cases} \quad (7)$$

for  $\mu_1$  and  $\mu_2$ , where  $\mu$  is the chemical potential and  $\alpha$  can be either vapor or liquid phase.

The phase diagram (pressure versus composition) of the binary mixture  $\text{CO}_2 + \text{CH}_4$  is extracted from Figure 4 and plotted in Figure 5, with results from experiment<sup>40</sup> and from the Gibbs ensemble technique.<sup>31</sup> The Gibbs ensemble technique is temperature-dependent. Its efficiency depends on the number of state points that are required to be calculated.

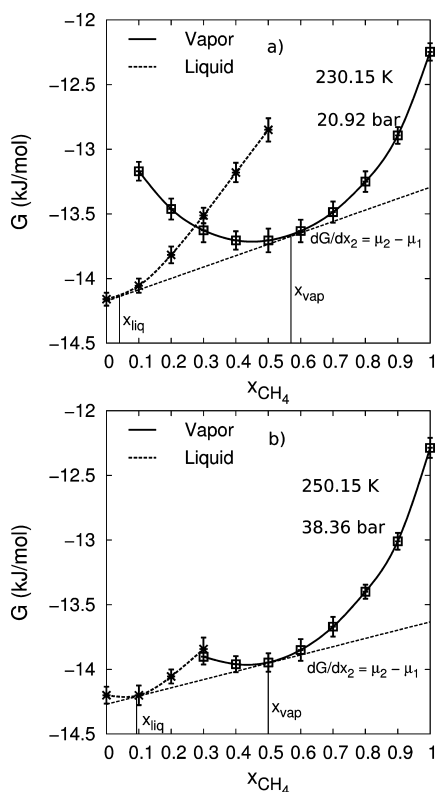


**Figure 4.** Gibbs free energy per particle versus  $\text{CH}_4$  composition for  $\text{CO}_2 + \text{CH}_4$ : (a) 230.15 K and 20.92 bar and (b) 250.15 K and 38.36 bar. The standard deviations are determined and shown as error bars by performing a set of 15 different simulations for each volume.

The energy partitioning method, on the other hand, is temperature-independent and does not suffer from this shortcoming. The vapor–liquid equilibrium properties computed using both simulation techniques agree well to within the statistical uncertainties of the simulations apart from a couple of points at low pressure. This discrepancy is, perhaps, due to the errors in fitting the curves and placing the double tangent lines. Reasonable agreement between experimental data and simulations is achieved for the liquid phase at both temperatures. However, the simulations slightly overestimate the solubility of  $\text{CH}_4$  in the vapor phase, which is due to the limitation of the force fields. This has been discussed in our previous work.<sup>31</sup>

Due to the finite size effect, the Gibbs ensemble technique cannot be used near the critical point. Using the energy partitioning method, we observe the occurrence of the critical point by constructing a plot of the Helmholtz free energy versus the volume of the system. Figure 6 shows such plots for mixtures of  $\text{CO}_2 + \text{CH}_4$  at 230.15 and 250.15 K. The critical point occurs when the second and third derivatives  $d^2F/dV^2$  are both zero, and the critical pressure is  $-dF/dV$  at the same point. The occurrence of the critical point is observed visually. The critical composition at 230.15 K is  $x_{\text{CH}_4} \approx 0.64$  and the critical pressure is approximately 70 bar. The critical composition at 250.15 K is  $x_{\text{CH}_4} \approx 0.55$ , and the critical pressure is approximately 81 bar. These results were obtained using mole fractions of  $\text{CH}_4$  separated by 0.02 (not shown in Figure 6 for clarity), and the uncertainties in the critical composition and pressure are estimated to be 0.02 and 5 bar, respectively. The critical pressure can also be extrapolated from

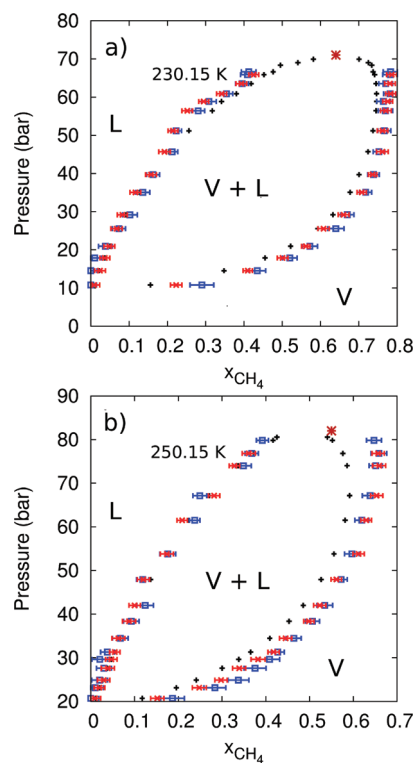


**Figure 5.** Phase diagram of the  $\text{CO}_2 + \text{CH}_4$  system at (a) 230.15 K and (b) 250.15 K. Energy partitioning method (squares with error bars) versus experimental data (pluses) and Gibbs ensemble technique (crosses with error bars). Stars indicate the critical points calculated from the energy partitioning method.

the simulated data by plotting  $p$  versus  $x_{\text{vap}} - x_{\text{liq}}$ . At the critical point,  $x_{\text{vap}} - x_{\text{liq}}$  is equal to zero. These results agree with those given above. The apparent critical points of a finite system depend on the system size,  $V$ . These parameters obey a scaling law behavior with  $V$ .<sup>41–45</sup> To investigate the sensitivity of the calculated critical points with the system size used, we have calculated the critical points (critical pressures and compositions) for systems with double and half of the size of the studied system. We found that the apparent critical pressures and  $\text{CH}_4$  mole fractions of small systems are slightly higher than those of bigger systems. However, these differences are still within the uncertainties of the estimation of the critical points.

Figure 7 shows the chemical potentials of each species in the mixture  $\text{CO}_2 + \text{CH}_4$  at the vapor–liquid equilibrium condition, calculated using eq 7. At both temperatures, the chemical potential of  $\text{CH}_4$  increases steeply while that of  $\text{CO}_2$  decreases gradually as the pressure increases. The gradient of the chemical potential of  $\text{CH}_4$  decreases as the pressure increases. This indicates that at the vapor–liquid equilibrium condition the chemical potential of  $\text{CH}_4$  is more sensitive to pressure than that of  $\text{CO}_2$  and that the solubility of  $\text{CH}_4$  in  $\text{CO}_2$  increases with the pressure.

The rate of change of the chemical potentials with respect to the pressure of a given species (species 1, for example) at two-phase equilibrium can be expressed in terms of the mole

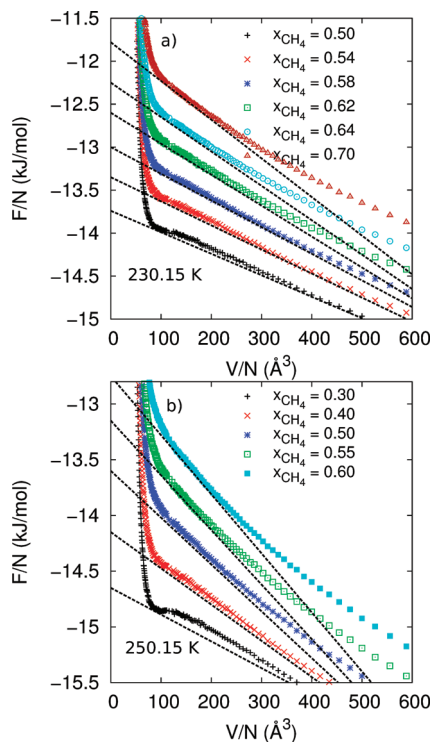


**Figure 6.** Helmholtz free energy per particle versus volume per particle of the mixture  $\text{CO}_2 + \text{CH}_4$  at different compositions at (a) 230.15 K and (b) 250.15 K. The standard errors are determined by performing a set of 15 different simulations for each volume. In most cases, the errors are between 0.4% and 0.7%. For the sake of clarity, the plots in (a) at the compositions of  $\text{CH}_4$  equal to 0.5, 0.54, 0.58, 0.62, and 0.64 are offset by  $-1.0$ ,  $-0.8$ ,  $-0.6$ ,  $-0.4$ , and  $-0.2$  kJ/mol, respectively. The plots in (b) at the compositions of  $\text{CH}_4$  equal to 0.3, 0.4, 0.5, and 0.55 are offset by  $-0.8$ ,  $-0.6$ ,  $-0.4$ , and  $-0.2$  kJ/mol, respectively.

fraction of the other species in both phases and the molar volume ( $v$ ) of each phase as

$$\frac{d\mu_1}{dp} = \frac{x_2^{\beta} v^{\alpha} - x_2^{\alpha} v^{\beta}}{x_2^{\beta} - x_2^{\alpha}} \quad (8)$$

Thus, since the mole fractions and the volumes of each phase are known (Figures 3 and 4),  $d\mu_1/dp$  can be calculated. For example,  $d\mu_{\text{CH}_4}/dp$  at 230.15 K and 29.16 bar is about  $870 \text{ cm}^3/\text{mol}$  and that calculated using eq 8 gives  $890 \text{ cm}^3/\text{mol}$ . The difference between these two numbers comes from the uncertainties in placing the tangent line. Equation 8 can also be used to interpret the behavior of the chemical potentials shown in Figure 7. The rate of change of the chemical potential of  $\text{CH}_4$  with respect to the pressure is  $(x_{\text{CO}_2}^{\text{liq}} v^{\text{vap}} - x_{\text{CO}_2}^{\text{vap}} v^{\text{liq}})/(x_{\text{CO}_2}^{\text{liq}} - x_{\text{CO}_2}^{\text{vap}})$ . Since the molar volume of vapor is larger than that of liquid and the mole fraction of  $\text{CO}_2$  in the liquid is always greater than in the vapor, this quantity is always positive. At low pressure, the molar volume of the vapor phase is much larger than that of the liquid phase, and this results in a steep slope. As the pressure increases, the volume of the vapor phase get closer to each other, which decreases the magnitude of  $d\mu_{\text{CH}_4}/dp$ . This is observed from Figure 7. A similar analysis can be done for  $d\mu_{\text{CH}_4}/dp$ , which equals  $(x_{\text{CH}_4}^{\text{liq}} v^{\text{vap}} - x_{\text{CH}_4}^{\text{vap}} v^{\text{liq}})/(x_{\text{CH}_4}^{\text{liq}} - x_{\text{CH}_4}^{\text{vap}})$ . Although the volume of the vapor phase is much greater

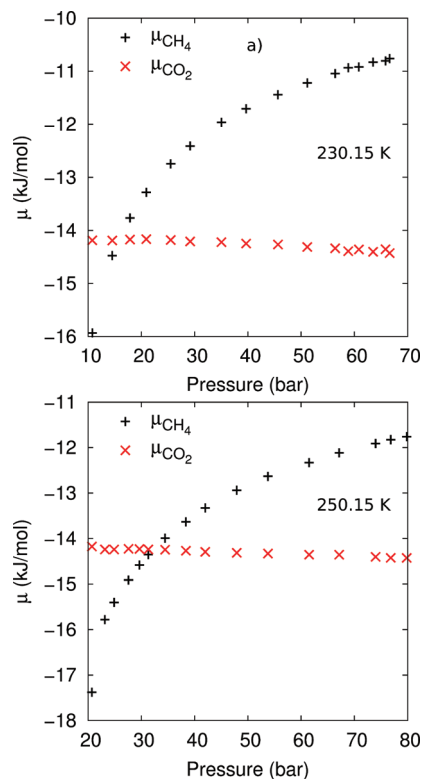


**Figure 7.** Chemical potentials of each species in the mixture  $\text{CO}_2 + \text{CH}_4$  at the vapor–liquid equilibrium condition versus pressure at (a) 230.15 K and (b) 250.15 K.

than that of the liquid phase, the mole fraction of  $\text{CH}_4$  in the liquid phase is smaller than that in the vapor phase. Therefore,  $x_{\text{CH}_4}^{\text{liq}} v^{\text{vap}} - x_{\text{CH}_4}^{\text{vap}} v^{\text{liq}}$  is positive, while  $x_{\text{CH}_4}^{\text{liq}} - x_{\text{CH}_4}^{\text{vap}}$  is negative. Thus,  $d\mu_{\text{CH}_4}/dp$  is negative, which is observed in Figure 7b.

## 5. CONCLUSION

In this paper, we have calculated the density of states, partition function, free energy, and chemical potential of the binary mixture  $\text{CO}_2 + \text{CH}_4$  using an energy partitioning MC technique. The Gibbs free energy of the binary mixture is computed as a function of the volume and the composition. Knowing the Gibbs free energy allows us to predict the vapor–liquid equilibrium properties, which agree quite well with experimental data and simulations using the Gibbs ensemble technique. One of the advantages of the energy partitioning method is that it allows us to observe the occurrence of the critical composition by constructing plots of the Helmholtz free energy versus the volume. We also obtain the chemical potentials of each species in the mixture directly. These quantities are useful, but difficult to compute using other methods. At the vapor–liquid equilibrium condition, we find that the rate of change of the chemical potentials with respect to pressure of  $\text{CH}_4$  increases significantly, whereas that of  $\text{CO}_2$  slightly decreases. The chemical potential of  $\text{CH}_4$  varies significantly with pressure, while that of  $\text{CO}_2$  does not vary much. This is understandable in terms of the composition and the volume of both phases.

The energy partitioning method can be applied to other binary mixtures and can be easily extended to study ternary mixtures and the free energy of transfer between two solvent phases. Standard methods for measuring free energy differences,

such as thermodynamic integration and free energy perturbation, are not directly applicable to calculations of the free energy of transfer.<sup>46</sup> A combination of the Gibbs ensemble method, Widom's test particle<sup>47</sup> and the configurational biased MC technique<sup>48,49</sup> have been used to tackle this problem for alkanes.<sup>46,50</sup> Using the energy partitioning method, the free energy of transfer could be obtained from the chemical potential. Since the method gives access to the free energy, it will be useful in many other applications. Also, the method can be extended to study systems with discrete energy levels, for which there is also a large number of applications.

## AUTHOR INFORMATION

### Corresponding Author

\*E-mail: hainam.do@nottingham.ac.uk.

### Notes

The authors declare no competing financial interest.

## ACKNOWLEDGMENTS

We thank the University of Nottingham High Performance Computing facility for providing computer resources and the Engineering and Physical Sciences Research Council (EPSRC) for funding (Grant No. EP/E06082X). We thank Prof. Martyn Poliakoff and Dr. Jie Ke for useful discussions. H.D. is grateful to the EPSRC for a Ph.D. Plus Fellowship.

## REFERENCES

- (1) Henderson, D.; Barker, J. A. *Phys. Rev. A* **1970**, *1*, 1266–1267.
- (2) Zwanzig, R. W. *J. Chem. Phys.* **1954**, *22*, 1420–1426.
- (3) Frenkel, D.; Smit, B. *Understanding Molecular Simulation: from Algorithms to Applications*, 2nd ed.; Academic Press: San Diego, CA, **2002**.
- (4) Hansen, J.; Verlet, L. *Phys. Rev.* **1969**, *184*, 151–161.
- (5) Head, M. S.; Given, J. A.; Gilson, M. K. *J. Phys. Chem. A* **1997**, *101*, 9241–9246.
- (6) Krisvov, S. V.; Karplus, M. J. *J. Chem. Phys.* **2002**, *117*, 10894–10903.
- (7) Evans, D. A.; Wales, D. J. *J. Chem. Phys.* **2003**, *119*, 9947–9955.
- (8) White, R. P.; Meirovitch, H. *J. Chem. Phys.* **2003**, *119*, 12096–12105.
- (9) White, R. P.; Meirovitch, H. *Proc. Natl. Acad. Sci. U.S.A.* **2004**, *101*, 9235–9240.
- (10) Meirovitch, H. *Phys. Rev. A* **1985**, *32*, 3709–3715.
- (11) Meirovitch, H. *J. Chem. Phys.* **1999**, *111*, 7215–7224.
- (12) Tyka, M. D.; Clarke, A. R.; Sessions, R. B. *J. Phys. Chem. B* **2006**, *110*, 17212–17220.
- (13) Tyka, M. D.; Sessions, R. B.; Clarke, A. R. *J. Phys. Chem. B* **2007**, *111*, 9571–9580.
- (14) Ytreberg, F. M.; Zuckerman, D. M. *J. Chem. Phys.* **2006**, *124*, 104105–104114.
- (15) Zhang, X.; Mamonov, A. B.; Zuckerman, D. M. *J. Comput. Chem.* **2009**, *30*, 1680–1691.
- (16) Bhatt, D.; Zuckerman, D. M. *J. Phys. Chem.* **2009**, *131*, 214110–214120.
- (17) Torrie, G. M.; Valleau, J. P. *J. Comput. Phys.* **1977**, *23*, 187–199.
- (18) Ferrenberg, A. M.; Swendsen, R. H. *Phys. Rev. Lett.* **1988**, *61*, 2635–2638.
- (19) Ferrenberg, A. M.; Swendsen, R. H. *Phys. Rev. Lett.* **1989**, *63*, 1195–1198.
- (20) Wang, J. S.; Tay, T. K.; Swendsen, R. H. *Phys. Rev. Lett.* **1999**, *82*, 476–479.
- (21) Berg, B.; Neuhaus, T. *Phys. Lett. B* **1991**, *267*, 249–253.
- (22) Wang, F. G.; Landau, D. P. *Phys. Rev. Lett.* **2001**, *86*, 2050–2053.
- (23) Ganzenmuller, G.; Camp, P. J. *J. Chem. Phys.* **2007**, *127*, 154504–154513.
- (24) Shell, M. S.; Debenedetti, P. G.; Panagiotopoulos, A. Z. *Phys. Rev. E* **2002**, *66*, 56703–56712.
- (25) Shell, M. S.; Debenedetti, P. G.; Panagiotopoulos, A. Z. *J. Chem. Phys.* **2003**, *119*, 9406–9411.
- (26) Yan, Q.; Faller, R.; de Pablo, J. J. *J. Chem. Phys.* **2002**, *116*, 8745–8749.
- (27) Do, H.; Hirst, J. D.; Wheatley, R. J. *J. Chem. Phys.* **2011**, *135*, 174105–174112.
- (28) Oakley, M. T.; Wheatley, R. J. *J. Chem. Phys.* **2009**, *130*, 34110–34119.
- (29) Oakley, M. T.; Do, H.; Wheatley, R. J. *Fluid Phase Equilib.* **2009**, *290*, 48–54.
- (30) Oakley, M. T.; Do, H.; Hirst, J. D.; Wheatley, R. J. *J. Chem. Phys.* **2011**, *134*, 114518–114525.
- (31) Do, H.; Wheatley, R. J.; Hirst, J. D. *J. Phys. Chem. B* **2010**, *114*, 3879–3886.
- (32) Do, H.; Wheatley, R. J.; Hirst, J. D. *Phys. Chem. Chem. Phys.* **2010**, *12*, 13266–13272.
- (33) Do, H.; Wheatley, R. J.; Hirst, J. D. *Phys. Chem. Chem. Phys.* **2011**, *13*, 15708–15713.
- (34) Poliakoff, M.; King, P. *Nature* **2001**, *412*, 125–125.
- (35) Skarmoutsos, I.; Hunt, P. A. *J. Phys. Chem. B* **2010**, *114*, 17120–17127.
- (36) Harris, J. G.; Yung, K. H. *J. Phys. Chem.* **1995**, *99*, 12021–12024.
- (37) Vorholz, J.; Harismeadis, V. I.; Rumpf, B.; Panagiotopoulos, A. Z.; Maurer, G. *Fluid Phase Equilib.* **2000**, *170*, 203–234.
- (38) Liu, Y.; Panagiotopoulos, A. Z.; Debenedetti, P. G. *J. Phys. Chem. B* **2011**, *115*, 6629–6635.
- (39) Chen, B.; Siepmann, J. I. *J. Phys. Chem. B* **1999**, *103*, 5370–5379.
- (40) Wei, M. S. W.; Brown, T. S.; Kidnay, A. J.; Sloan, E. D. *J. Chem. Eng. Data* **1995**, *40*, 726–731.
- (41) Chen, J. H.; Fisher, M. E.; Nickel, B. G. *Phys. Rev. Lett.* **1982**, *48*, 630–634.
- (42) Ferrenberg, A. M.; Landau, D. P. *Phys. Rev. B* **1991**, *44*, 5081–5091.
- (43) Wilding, N. B. *Phys. Rev. E* **1995**, *52*, 602–611.
- (44) Wilding, N. B. *Phys. Rev. E* **1997**, *55*, 6624–6631.
- (45) Potoff, J. J.; Panagiotopoulos, A. Z. *J. Chem. Phys.* **1998**, *109*, 10914–10920.
- (46) Martin, M. G.; Siepmann, J. I. *J. Am. Chem. Soc.* **1997**, *119*, 8921–8924.
- (47) Widom, B. *J. Chem. Phys.* **1963**, *39*, 2808–2812.
- (48) Siepmann, J. I.; Frenkel, D. *Mol. Phys.* **1992**, *68*, 931–950.
- (49) Frenkel, D.; Mooji, G. C. A. M.; Smit, B. *J. Phys.: Condens. Matter* **1992**, *4*, 3053–3076.
- (50) Martin, M. G.; Siepmann, J. I. *Theor. Chem. Acc.* **1998**, *99*, 347–350.